Dose Painting in Radiotherapy for Head and Neck Squamous Cell Carcinoma: Value of Repeated Functional Imaging with ^{18}F-FDG PET, ^{18}F-Fluoromisonidazole PET, Diffusion-Weighted MRI, and Dynamic Contrast-Enhanced MRI

Piet Dirix[1], Vincent Vandecaveye[2], Frederik De Keyzer[2], Sigrid Stroobants[3], Robert Hermans[2], and Sandra Nuyts[1]

[1]Department of Radiation Oncology, Leuvens Kankerinstituut, University Hospitals Leuven, Leuven, Belgium; [2]Department of Radiology, Leuvens Kankerinstituut, University Hospitals Leuven, Leuven, Belgium; and [3]Department of Nuclear Medicine, Leuvens Kankerinstituut, University Hospitals Leuven, Leuven, Belgium

The purpose of this work was to evaluate the potential of functional imaging with ^{18}F-FDG PET, ^{18}F-fluoromisonidazole PET, diffusion-weighted MRI, and dynamic contrast-enhanced MRI to provide an appropriate and reliable biologic target for dose painting in radiotherapy for head and neck squamous cell carcinoma (HNSCC). **Methods:** Fifteen patients with locally advanced HNSCC, treated with concomitant chemoradiotherapy, were prospectively enrolled in a bioimaging protocol. Sequential PET (^{18}F-FDG and ^{18}F-fluoromisonidazole) and MRI (T1, T2, dynamic enhanced, and diffusion-weighted sequences) were performed before, during, and after radiotherapy. **Results:** Median follow-up was 30.7 mo (range, 6.3–56.3 mo); in 7 patients, disease recurred. Disease-free survival correlated negatively with the maximum tissue-to-blood ^{18}F-fluoromisonidazole ratio (T/B_{max}) on the baseline ^{18}F-fluoromisonidazole scan ($P = 0.04$), with the size of the initial hypoxic volume ($P = 0.04$), and with T/B_{max} on the ^{18}F-fluoromisonidazole scan during treatment ($P = 0.02$). All locoregional recurrences were within the ^{18}F-FDG–avid regions on baseline ^{18}F-FDG PET; 3 recurrences mapped outside the hypoxic volume on baseline ^{18}F-fluoromisonidazole PET. Lesions (primary tumor and lymph nodes) where a locoregional recurrence developed during follow-up had significantly lower apparent diffusion coefficients on diffusion-weighted MRI during week 4 of radiotherapy (0.0013 vs. 0.0018 mm^2/s, $P = 0.01$) and at 3 wk after treatment (0.0014 vs. 0.0018 mm^2/s, $P = 0.01$) and a significantly higher initial slope on baseline dynamic enhanced MRI (26.2 vs. 17.5/s, $P = 0.03$) than did lesions that remained controlled. **Conclusion:** These results confirm the added value of ^{18}F-FDG PET and ^{18}F-fluoromisonidazole PET for radiotherapy planning of HNSCC and suggest the potential of diffusion-weighted and dynamic enhanced MRI for dose painting and early response assessment.

Received Jan. 27, 2009; revision accepted Mar. 16, 2009.
For correspondence or reprints contact: Piet Dirix, Department of Radiation Oncology, Leuvens Kankerinstituut (LKI), University Hospitals Leuven, Campus Gasthuisberg, Herestraat 49 B-3000, Leuven, Belgium.
E-mail: piet.dirix@uzleuven.be

Key Words: head and neck cancer; radiotherapy; PET; MRI
J Nucl Med 2009; 50:1020–1027
DOI: 10.2967/jnumed.109.062638

Since its introduction in the previous decade, intensity-modulated radiotherapy has been widely applied in head and neck squamous cell carcinoma (HNSCC). This treatment method allows high-dose areas to be conformed tightly to the target volumes, with dose falling off steeply outside these regions. In the head and neck region, where malignant growth often lies near critical normal tissues, intensity-modulated radiotherapy has the potential to ensure sufficient target coverage while significantly reducing toxicity. Another promising application is the introduction of dose escalation to improve tumor control. As intensity-modulated radiotherapy permits lowering the dose to the organs at risk outside the target volume, the maximum dose becomes restricted by the presence of dose-limiting structures within the target volume, such as cartilage, connective tissue, nerves, and bone. It was therefore suggested that dose escalation should be targeted to areas of increased radioresistance in the tumor (*1*). Functional imaging, that is, modalities that offer information on factors that influence treatment outcome (e.g., tumor burden, proliferation, and hypoxia), is expected to provide the biologic target volume for such dose painting (*2,3*).

The most commonly used functional imaging modality for radiotherapy planning is undoubtedly ^{18}F-FDG PET (*4*). In HNSCC, ^{18}F-FDG PET has a clear impact on both primary tumor delineation and cervical lymph node staging (*5,6*). Results from several trials suggest that pretreatment ^{18}F-FDG uptake correlates with outcome in HNSCC

patients and can therefore indicate a valuable target for dose escalation (*7,8*).

Another promising PET tracer is ^{18}F-fluoromisonidazole, providing quantitative measurements of hypoxia, one of the main factors affecting treatment resistance in HNSCC. The group from the University of Washington was the first to determine the hypoxic fraction of tumors by using ^{18}F-fluoromisonidazole PET (*9*). Researchers from the same institution performed pretreatment ^{18}F-fluoromisonidazole PET on 73 HNSCC patients. Significant hypoxia was present in 58 patients (79%), and both the degree of hypoxia and the size of the hypoxic volume were independent predictive factors for survival (*10*). These data imply that ^{18}F-fluoromisonidazole PET can be used to estimate the burden of hypoxia in HNSCC and can provide a promising target for dose painting (*11,12*).

Diffusion-weighted (DW) MRI is able to detect molecular diffusion, that is, the Brownian motion of water molecules in tissues. DW images are obtained by applying pairs of magnetic field gradients around the refocusing pulse of a T2-weighted sequence. Movement of the tissue water molecules between the 2 gradients results in dephasing, depicted as signal loss (*13*). This signal loss will be proportional to the amount of water molecule movement and the strength of the gradients (b-value). By repeating the sequence with different b-values, one can quantify the observed signal loss using the apparent diffusion coefficient. Value has been shown for DW MRI in detecting recurrences after radiotherapy, in lymph node staging of HNSCC, and in evaluating radiation-induced xerostomia (*14–16*). Preclinical and clinical data indicate several potential roles for DW MRI, including determination of lesion aggressiveness and monitoring response to therapy (*17*).

Dynamic contrast-enhanced MRI assesses changes in signal intensity after the intravenous injection of a paramagnetic contrast agent that reduces the T1 (longitudinal relaxation time) value of blood and thus enhances signal intensity on T1-weighted imaging. Serial T1-weighted imaging samples the blood signal at intervals of a few seconds for up to several minutes after injection (*18*). The temporal changes in signal intensity obtained by dynamic enhanced MRI are related to the underlying permeability and perfusion of the tumor microenvironment and to the interstitial pressures within the tumor, all of which are known to influence treatment response (*19*).

Because biologically optimized intensity-modulated radiotherapy represents a promising approach to improving the therapeutic index of radiotherapy for HNSCC, the purpose of this prospective study was to evaluate the potential of functional imaging with ^{18}F-FDG PET, ^{18}F-fluoromisonidazole PET, DW MRI, and dynamic enhanced MRI to provide an appropriate and reliable biologic target for dose painting.

MATERIALS AND METHODS

Study Design

In this prospective study, 15 patients with locally advanced HNSCC scheduled for primary radiotherapy underwent repeated imaging with PET/CT before, during, and after treatment between January 2004 and May 2006. Since April 2005, when the MRI acquisition protocol became fully validated, the last 8 patients (patients 8–15) also underwent MRI.

Patient and tumor characteristics are summarized in Table 1. There were 13 male and 2 female patients, with a median age of 57 y (range, 46–61 y). The patients had squamous cell carcinoma of the oropharynx (n = 6), larynx (n = 5), hypopharynx (n = 3), or oral cavity (n = 1). Treatment was decided by a multidisciplinary team according to institutional guidelines and consisted of concomitant chemoradiotherapy in all 15 patients. Radiotherapy was delivered according to a hybrid fractionation schedule: 20 daily fractions of 2 Gy (40 Gy) followed by 20 fractions of 1.6 Gy twice daily (32 Gy) to a total dose of 72 Gy, as described previously (*20*). Patients also received cisplatinum (100 mg/m^2) intravenously, on the first day of weeks 1 and 4 (*20*). The study protocol was approved by the local ethics committee; informed consent was obtained from all patients.

The treatment and imaging protocol is shown in Figure 1. The patients underwent ^{18}F-FDG PET/CT before the start of radiother-

TABLE 1. Patient and Tumor Characteristics

Patient no.	Primary tumor site	Age (y)	Sex	cT	cN	GTV_{CT} (mL)	Disease recurrence
1	Hypopharynx	59	M	4a	1	46.38	No
2	Hypopharynx	58	F	1	2b	17.82	No
3	Larynx	48	M	3	0	23.06	No
4	Oropharynx	57	M	3	2b	19.08	DM
5	Oropharynx	48	M	2	2c	16.96	LR + DM
6	Oropharynx	60	M	2	2c	19.9	LR + DM
7	Oropharynx	48	M	4a	1	42.3	No
8	Oropharynx	55	M	4a	1	28.01	LR + DM
9	Oropharynx	58	M	2	2b	14.53	LR + DM
10	Larynx	58	M	3	2b	68.34	No
11	Larynx	60	M	4a	2c	20.47	LR
12	Hypopharynx	46	M	4a	1	19.37	No
13	Larynx	51	F	4a	2c	33.82	No
14	Larynx	61	M	1	2c	84.97	DM
15	Oral cavity	55	M	4a	2c	48.51	No

cT = clinical T classification; cN = clinical N classification; DM = distant metastases; LR = locoregional recurrence.

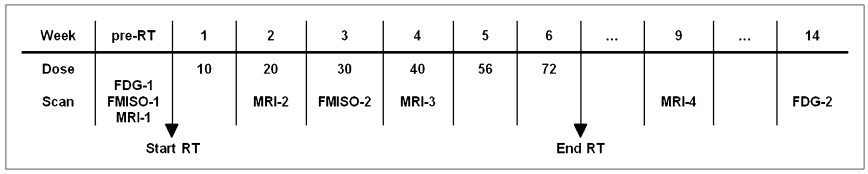

FIGURE 1. Treatment and imaging protocol.

apy (median interval, 5 d; range, 0–18 d) and 8 wk after the end of treatment (median interval, 58 d; range, 50–65 d). The patients also underwent ^{18}F-fluoromisonidazole PET/CT before the start of treatment (median interval, 7 d; range, 1–14 d), although 3 scans could not be interpreted for technical reasons (patients 3, 7, and 12). The ^{18}F-fluoromisonidazole PET/CT scan was repeated during the fourth week after the start of radiotherapy (median interval, 28 d; range, 16–42 d) to evaluate residual hypoxia. The last 8 patients (patients 8–15) underwent MRI before the start of treatment (median interval, 10 d; range, 7–21 d), during the second week (median interval, 15 d; range, 14–22 d) and fourth week (median interval, 29 d; range, 27–31 d) after the start of radiotherapy, and 3 wk after the end of treatment (median interval, 26 d; range, 12–41 d). The DW and dynamic enhanced MRI scans of patient 14 could not be interpreted for technical reasons.

After treatment, patients were regularly followed at the multidisciplinary outpatient clinic: every 2 mo the first 2 y after treatment, every 3 mo the third year, every 4 mo the fourth year, every 6 mo the fifth year, and then every year. Response evaluation consisted of physical examination and CT at 2–3 mo after treatment. Thereafter, CT was performed yearly or at the discretion of the treating oncologist (*20*).

Image Acquisition

CT was performed for conformal treatment-planning purposes in a clinical routine setting: serial slices 3 mm thick from the head to the clavicles were obtained after intravenous injection of a contrast agent.

Investigational PET/CT was performed on a Biograph integrated PET/CT scanner (Siemens) with an intrinsic resolution of 4 mm in full width at half maximum. Patients were scanned supine on a flat-top couch insert. The head, neck, and shoulders were immobilized using a thermoplastic mask (Posicast; Sinmed) prepared during a radiotherapy simulation session and used throughout treatment. ^{18}F-FDG was prepared, and a mean of 358 MBq (range, 240–428 MBq) was administered intravenously to patients who had been fasting for at least 6 h. At 45–60 min after injection, ^{18}F-FDG PET/CT was performed.

The ^{18}F-fluoromisonidazole PET/CT data were acquired at 120–160 min after intravenous injection of 370 MBq of ^{18}F-fluoromisonidazole; no fasting period was required. The ^{18}F-fluoromisonidazole emission data were corrected for attenuation, scatter, and random counts and then were iteratively reconstructed using standard clinical ^{18}F-FDG parameters. Venous blood samples were obtained immediately after the ^{18}F-fluoromisonidazole PET/CT session. Measured aliquots of each blood sample were counted in triplicate, and the net counting rates were converted to activity concentrations (Bq/mL) and then decay-corrected to the time of injection.

The MRI protocol has previously been detailed (*14,15*). The examinations were performed on a 1.5-T scanner (Magnetom Sonata Vision; Siemens) using a combination of a standard head coil and a 2-channel phased-array neck coil. First, transverse T2-weighted (repetition time [TR]/echo time [TE], 3,080/106 ms) and T1-weighted (TR/TE, 775/8.3 ms) turbo spin-echo sequences were acquired in an imaging block of 48 slices with a 4-mm slice thickness and a field of view of 20 × 25 cm. An echoplanar DW MRI sequence was then acquired using identical geometry, a TR/TE of 7,400/84 ms, and b-values of 0, 50, 100, 500, 750, and 1,000 s/mm^2. Dynamic enhanced sequences were acquired using a 3-dimensional T1-weighted gradient-echo sequence with fat saturation (volumetric interpolated breath-hold examination). The dynamic enhanced MRI sequence consisted of 48 slices, a 4-mm slice thickness, a 22.5 × 30 cm field of view, a TR/TE of 4.3/1.6 ms, and a run time of 8.4 s. After 5 baseline dynamic enhanced MRI runs, a single-dose intravenous bolus of gadobenate dimeglumine (Multihance; Bracco) was injected, and the sequence was continually repeated for 20 more dynamic enhanced MRI runs. Coronal or sagittal T1-weighted turbo spin-echo sequences were added, depending on tumor location.

Image Analysis

Planning-CT images were transferred to a commercial planning workstation (Eclipse; Varian Inc.). The gross tumor volume was delineated anatomically on CT images (GTV_{CT}) by the treating radiation oncologist, and these volumes were retrospectively retrieved for comparison with the investigational imaging techniques.

The GTV_{FDG} was the result of automatic segmentation of the ^{18}F-FDG PET images, based on the source-to-background ratio (*21*). The standardized uptake value (SUV), an index of glucose metabolism that equals the ^{18}F-FDG uptake in each pixel normalized by the injected dose and body weight, was calculated in each tumor volume. A region of interest was centered in the area of highest tumor ^{18}F-FDG uptake (primary tumor or lymph nodes), and the maximal SUV (SUV_{max}) was recorded.

The hypoxic volume on ^{18}F-fluoromisonidazole PET was defined as the pixels with a tissue-to-blood ^{18}F-fluoromisonidazole ratio of 1.2 or more (*22*). In each tumor volume, we also located the pixel with the maximum tissue-to-blood ratio (T/B_{max}) and recorded this variable for statistical analysis. Although the hypoxic volume evaluates the volume of tumor that has crossed the threshold for significant hypoxia, the T/B_{max} depicts the magnitude of hypoxia. To transfer contours of structures drawn on the PET/CT images to the planning-CT images, the CT data from the PET/CT study were registered with the planning-CT data using the software available in the radiotherapy planning workstation.

Both T2-weighted and contrast-enhanced T1-weighted sequences were transferred to the radiotherapy planning system, and corresponding tumor volumes (GTV_{T2} and GTV_{T1}, respectively) were manually delineated by a radiation oncologist and a radiologist working in consensus while unaware of the other imaging data.

The DW and dynamic enhanced images were transferred to an independent Linux workstation with dedicated software (Biomap; Novartis). On the DW images with a b-value of 0 s/mm^2, the primary tumor and all identifiable lymph nodes (GTV_{DW}) were contoured. These were then copied and pasted onto the images acquired with other b-values. From the signal intensity averages

per region of interest and per b-value, apparent diffusion coefficients were calculated (*14–16*).

For evaluation of the dynamic enhanced images, pixelwise signal-intensity curves (SIC) were calculated from the perfusion image series using the following formula: $SIC_i = (I_i - I_0)/I_0$, for all time points i, where I_i is the signal intensity at perfusion imaging at time point i, and I_0 is the signal intensity at baseline perfusion imaging. Further evaluation was performed by calculating the slope of the contrast enhancement–time curve at the time point of maximal contrast agent inflow, which was defined as the initial slope: max[d(SIC)/dt].

Each local or regional recurrence volume was delineated on the diagnostic CT scan demonstrating the relapse. That CT scan was then registered to the planning-CT scan to characterize the failure as being in the field, marginal, or out of the field (*23*). This step also allowed us to determine the exact correlation of the recurrence volume with the initial GTV_{FDG} and the hypoxic volume.

Statistical Analysis

Patient characteristics were recorded at the start of treatment. Follow-up data were retrospectively collected: information was sought on the date of the first locoregional recurrence, distant metastasis, or death. The close-out date for survival analysis was August 1, 2008. The statistical data were analyzed using the software package Statistica 8 (StatSoft Inc.). Cumulative disease-free survival rates were calculated using the Kaplan–Meier product-limited (actuarial) method. To compare apparent diffusion coefficients between recurring and controlled regions of interest (primary tumor and lymph nodes), we used an unpaired 2-tailed Student *t* test. A *P* value of less than 0.05 was considered statistically significant.

RESULTS

Imaging Results

Before radiotherapy, the mean GTV_{CT} was 33.6 mL (range, 14.5–85.0 mL), the mean GTV_{T1} was 40.3 mL (range, 14.5–101.3 mL), and the mean GTV_{T2} was 34.6 mL (range, 12.4–85.3 mL). There was an excellent correlation between GTV_{CT} and GTV_{T1} ($R^2 = 0.98$) and between GTV_{CT} and GTV_{T2} ($R^2 = 0.96$) before the start of radiotherapy. During treatment, there was considerable shrinkage of the anatomic tumor volume. During the second week of radiotherapy, the mean GTV_{T1} was 28.7 mL (range, 7.3–95.7 mL) and the mean GTV_{T2} was 24.9 mL (range, 4.6–74.9 mL): a decrease of 28.8% and 28.1%, respectively. During the fourth week of radiotherapy, the mean GTV_{T1} was 19.2 mL (range, 1.1–65.9 mL) and the mean GTV_{T2} was 16.4 mL (range, 1.1–58.2 mL), so that 47.6% and 47.4%, respectively, of the initial volume remained. There was an excellent correlation between GTV_{T1} and GTV_{T2} before radiotherapy ($R^2 = 0.99$) and during the second ($R^2 = 0.98$) and fourth ($R^2 = 0.98$) weeks of treatment.

On baseline ^{18}F-FDG PET, the mean GTV_{FDG} was 18.7 mL (range, 5.2–81.1 mL) and the mean SUV_{max} was 9.81 (range, 6.6–17.5). The GTV_{FDG} was significantly smaller than the GTV_{CT} on a paired 2-tailed Student *t* test ($P = 0.0005$). On baseline ^{18}F-fluoromisonidazole PET, the mean hypoxic volume was 4.1 mL (range, 0–16.6 mL) and the mean T/B_{max} was 1.5 (range, 1.1–2.1). There was little residual hypoxia on the second ^{18}F-fluoromisonidazole PET scans (Table 2): the mean hypoxic volume was 0.3 mL (range, 0–3.2 mL) and the mean T/B_{max} was 1.2 (range, 1.0–1.6).

On baseline DW MRI, the mean GTV_{DW} was 14.8 mL (range, 4.8–36.4 mL), significantly smaller than the GTV_{CT} on a paired 2-tailed Student *t* test ($P = 0.004$). During treatment, considerable shrinkage of the tumor volume was seen on DW MRI. During the second week of radiotherapy, the mean GTV_{DW} was 5.1 mL (range, 0.8–17.7 mL), and during the fourth week, the mean GTV_{DW} was 1.4 mL (range, 0–6.3 mL). At all time points before and during treatment, the GTV_{DW} was significantly smaller than the GTV_{T1} ($P < 0.01$) and the GTV_{T2} ($P < 0.01$) on a paired 2-tailed Student *t* test.

At 3 wk after treatment, the mean GTV_{T1} was 5.9 mL (range, 0–13.6 mL) and the mean GTV_{T2} was 3.3 mL (range, 0–9.0 mL). On DW MRI, apparent diffusion coefficient calculations showed residual disease in 3 patients (mean

TABLE 2. PET Data

	^{18}F-FDG-1		^{18}F-fluoromisonidazole-1		^{18}F-fluoromisonidazole-2		
Patient no.	GTV_{FDG} (mL)	SUV_{max}	Hypoxic volume (mL)	T/B_{max}	Hypoxic volume (mL)	T/B_{max}	^{18}F-FDG-2 response
1	25.74	8.00	6.4	1.59	0.09	1.42	Complete response
2	6.07	9.41	0.9	1.38	0.03	1.24	Complete response
3	8.13	17.46	—	—	0	0.96	Complete response
4	9.29	10.85	6.74	1.80	0	1.23	Complete response
5	10.09	8.25	0.02	1.25	0	1.00	Complete response
6	11.07	13.17	9.32	2.09	0	1.17	Residual disease
7	22.21	14.84	—	—	0	1.09	Complete response
8	23.42	6.98	6.1	1.51	3.23	1.61	Residual disease
9	15.01	9.53	0	1.17	0.85	1.38	Complete response
10	25.39	11.80	0	1.23	0	1.03	Complete response
11	15.1	8.25	3.74	1.51	0.03	1.28	Complete response
12	5.24	8.22	—	—	0	0.96	Complete response
13	16.7	6.80	0	1.13	0	1.00	Complete response
14	81.14	7.00	16.56	1.53	0	1.17	Complete response
15	6.33	6.59	0	1.16	0	1.08	Complete response

GTV_{DW}, 0.1 mL; range, 0–0.7 mL), in all of whom locoregional recurrence developed during follow-up. At 8 wk after the end of treatment, ^{18}F-FDG PET detected residual disease in 2 patients; locoregional recurrence developed in both.

Patterns of Failure

Median follow-up of all patients was 30.7 mo (range, 6.3–56.3 mo). Seven patients experienced disease recurrence after a median of 9.4 mo (range, 4.0–13.3 mo). At the time of analysis, 8 patients remained alive and disease-free, after a median follow-up time of 42.6 mo (range, 25.5–56.3 mo).

Actuarial disease-free survival correlated negatively with T/B_{max} on the baseline ^{18}F-fluoromisonidazole scan (P = 0.04, Fig. 2), with the size of the hypoxic volume on the baseline ^{18}F-fluoromisonidazole scan (P = 0.04), and with T/B_{max} on the second ^{18}F-fluoromisonidazole scan during radiotherapy (P = 0.02, Fig. 3). No significant correlation was observed between disease-free survival and the size of the initial GTV_{CT}, SUV_{max} on the baseline ^{18}F-FDG scan, the size of the initial GTV_{FDG}, or the size of the hypoxic volume on the second ^{18}F-fluoromisonidazole scan.

Five patients experienced local or regional recurrence during follow-up: 1 patient had a local relapse (patient 5), 2 patients had a regional relapse (patients 8 and 9), and 2 patients had a locoregional relapse (patients 6 and 11). There were 9 recurrent lesions (3 local and 6 regional) in total, with a mean recurrence volume of 12.7 mL (range, 0.7–36.4 mL). All recurrences were in-field, that is, within the GTV_{CT} and thus the high-dose region. Similarly, all recurrences were within the initial GTV_{T1} and GTV_{T2} and within the pretreatment GTV_{FDG} on baseline ^{18}F-FDG PET. Three recurrences mapped outside the pretreatment hypoxic volume on baseline ^{18}F-fluoromisonidazole PET.

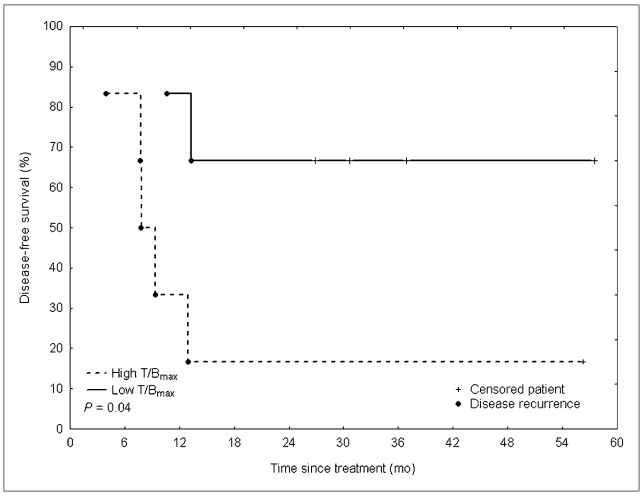

FIGURE 2. Actuarial disease-free survival according to T/B_{max} before radiotherapy (n = 12). High T/B_{max} is defined as a value greater than or equal to median of 1.45.

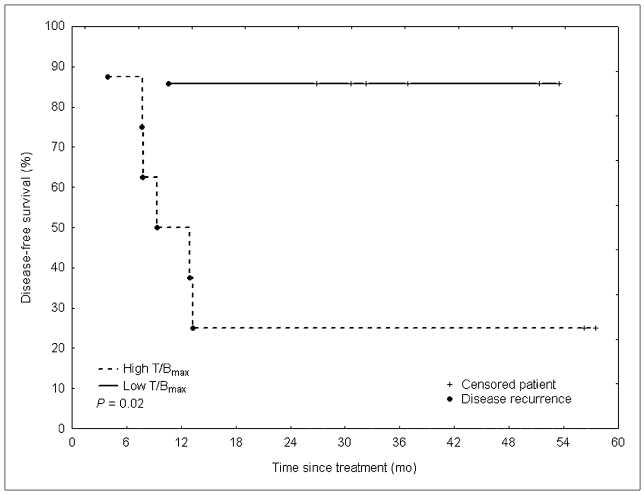

FIGURE 3. Actuarial disease-free survival according to T/B_{max} during radiotherapy (n = 15). High T/B_{max} is defined as a value greater than or equal to median of 1.17.

Lesions (i.e., primary tumor and lymph nodes) in which locoregional recurrence developed during follow-up had significantly lower apparent diffusion coefficients, both during the fourth week of radiotherapy (0.0013 vs. 0.0018 mm^2/s, P = 0.01) and at 3 wk after the end of treatment (0.0014 vs. 0.0018 mm^2/s, P = 0.01), than did lesions that remained controlled. Also, lesions with recurrence had a higher initial slope (26.2 vs. 17.5/s, P = 0.03) on baseline dynamic enhanced MRI.

DISCUSSION

In this prospective feasibility study, a multimodality imaging protocol with ^{18}F-FDG PET/CT, ^{18}F-fluoromisonidazole PET/CT, DW MRI, and dynamic enhanced MRI was applied to patients before, during, and after concomitant chemoradiotherapy for locally advanced HNSCC.

Regarding the anatomic imaging modalities, a good correlation was observed between volumes based on CT, T2-weighted turbo spin-echo MRI, or contrast-enhanced T1-weighted turbo spin-echo MRI, corroborating results from earlier reports (*5,24*). Although turbo spin-echo MRI provides a clear benefit in the delineation of tumors in the oral cavity and nasopharynx or at the base of skull, its routine use in pharyngolaryngeal tumors remains arguable (*25,26*). Reassessment with MRI during treatment did nonetheless demonstrate clear shrinkage of the tumor volume to approximately half its initial size at the fourth week, emphasizing the need for truly adaptive radiotherapy.

Our data confirmed the potential value of ^{18}F-FDG PET/CT for target volume delineation in patients with HNSCC (*4–8*). Although the GTV_{FDG}, based on a validated source-to-background algorithm, was significantly smaller than the anatomic tumor volume on CT, all locoregional failures occurred within the initial ^{18}F-FDG–avid volume. This finding suggests that the GTV_{FDG} within the GTV_{CT}

warrants escalated radiation doses (*8*). However, we did not find any correlation between the amount (size of the GTV_{FDG}) or the level (SUV_{max}) of ^{18}F-FDG uptake and disease-free survival, although this lack of correlation could be due to the limited number of patients. In fact, whereas the prognostic value of ^{18}F-FDG PET appears intuitively appealing, recent trials comparing SUV data to disease control in larger patient groups have reported conflicting results (*27–30*). In any case, it appears prudent not to use ^{18}F-FDG PET as the sole instrument for delineating gross tumor volume, since locoregional failures can occur outside the GTV_{FDG} (*8,30*). Pathology studies have convincingly demonstrated that no single imaging modality can depict all tumor extensions (*5*). However, MRI, CT, and ^{18}F-FDG PET can, when used together, add complementary data to improve tumor delineation.

Tumor hypoxia has been shown to be one of the major factors affecting treatment resistance in HNSCC (*31*). Noninvasive ^{18}F-fluoromisonidazole PET evaluating the gross disease can provide serial quantitative measurements of hypoxia, with potential prognostic implications (*9,10*). In our study, both the pretreatment amount of hypoxia (size of the hypoxic volume) and the level of hypoxia (T/B_{max}) correlated negatively with disease-free survival. This finding is consistent with the findings of earlier studies evaluating the significance of pretreatment ^{18}F-fluoromisonidazole uptake in HNSCC (*10,32,33*). To our knowledge, we are the first to report that the level of hypoxia (T/B_{max}) during radiotherapy correlates significantly with disease control. In 2 of 12 patients (patients 8 and 9, Table 2) with ^{18}F-fluoromisonidazole PET data available for the 2 time points, the T/B_{max} values actually increased. In both patients, locoregional recurrence and distant metastases developed during follow-up (Table 1), apparently confirming the expected negative prognostic impact of this finding. Similarly, Eschmann et al. observed increased ^{18}F-fluoromisonidazole uptake after administration of 30 Gy in 2 of 14 patients, both of whom experienced relapse (*34*).

A planning study by Popple et al. proposed that a modest boost dose (120%−150% of the primary dose) to regions of permanent hypoxia could significantly increase the probability of tumor control. However, only tumors with a geometrically stable hypoxic volume will have an improved control rate after dose escalation (*35*). Our data showed that considerable reoxygenation takes place during radiotherapy, as corresponds to observations by other groups (*34,36,37*). In our opinion, more work is required to elucidate the spatial–temporal evolution in intratumor distribution before single-time-point ^{18}F-fluoromisonidazole PET images can be used as a basis for hypoxia-targeting dose-escalation protocols.

Our preliminary results with DW MRI showed that lesions in which locoregional recurrence developed during follow-up had significantly lower apparent diffusion coefficients on scans during week 4 of radiotherapy and at 3 wk after treatment. Because a treatment-induced loss of tumor cells increases water mobility at the microscopic level, treatment response corresponds to an increase in apparent diffusion coefficients. On the other hand, remaining tumor cells can be detected as residually decreased apparent diffusion coefficients (*38*). Hypothetically, DW MRI could thus be used as a noninvasive tool to select patients who have a high risk of not achieving or maintaining locoregional control and therefore would benefit the most from treatment intensification, for example, boost-dose escalation to those subvolumes that harbor radioresistant clonogens (Fig. 4). Obviously, other approaches such as the addition of targeted agents or more toxic drugs could also be considered. Further validation of these preliminary results is currently ongoing in a much larger patient group.

Although the dynamic enhanced MRI scans during and after radiotherapy did not provide any information on treatment response, we did observe a significant correlation between initial slope on the baseline scan and disease control. Although preliminary, these results suggest that dynamic enhanced MRI can be used as a predictor of response to radiotherapy in HNSCC. Several studies have assessed the predictive role of pretreatment tumor enhancement, quantified as the initial slope or the peak enhancement, especially in gynecologic cancer. Most reports have shown that tumors with better enhancement are associated with better tumor regression and local control (*19*). This correlation is attributed to less hypoxia-related resistance in better perfused tumors. However, other studies have reported that high enhancement was associated with poor clinical outcome, as can be attributed to the increased aggressiveness of tumors with high angiogenic activity (*19,39*). These apparently contradictory findings are probably due to differences in patient population, tumor type, treatment, and clinical end-

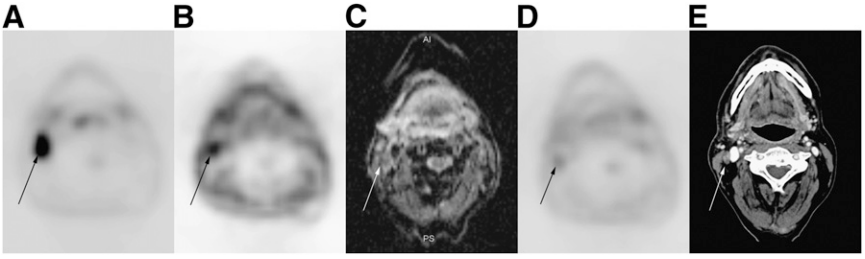

FIGURE 4. (A and B) Pretreatment ^{18}F-FDG PET showed metastatic adenopathy at level 2 (arrow) (A), which remained hypoxic on ^{18}F-fluoromisonidazole PET scan during RT treatment (week 4) (B). (C and D) This lymph node still had restricted apparent diffusion coefficient on DW MRI at 3 wk after end of radiotherapy (C) and remained suspect on ^{18}F-FDG PET at 8 wk after treatment (D). (E) Residual disease was confirmed in this node (patient 8).

point. Our results appear at odds with an earlier study using perfusion CT in a similar setting. Hermans et al. stratified 105 HNSCC patients according to the median perfusion value and found that patients with lower perfusion had a significantly higher local failure rate after radiotherapy (*40*).

It is evident that considerable further research and development is necessary before DW or dynamic enhanced MRI can be routinely used in radiotherapy planning. Interpretation of DW or dynamic enhanced MRI scans of the head and neck region is not straightforward, making the use of quantitative or semiquantitative measurements for target volume delineation absolutely necessary. However, this necessity is also one of the strengths of the technique, since a straightforward cutoff value would allow simple and reliable differentiation, potentially eliminating both intra- and interobserver variability (*15*). Also, DW or dynamic enhanced MRI scans have a nonnegligible nonaffine distortion, making fusion with planning-CT images difficult. Because of the low signal-to-noise ratio and the high level of deformation in DW and dynamic enhanced MRI, automatic nonrigid coregistration algorithms based on mutual information do not have enough information for accurate coregistration. Therefore, semiautomatic alterations of this algorithm have to be developed to provide the additional information required. Ultimately, successful introduction of functional imaging into clinical routine will likely depend on an improved standardization of imaging technique, interpretation, and registration.

CONCLUSION

These results confirm the added value of ^{18}F-FDG PET and ^{18}F-fluoromisonidazole PET for planning radiotherapy of HNSCC, and they suggest the potential of DW and dynamic enhanced MRI for dose painting and early response assessment. We are currently validating these preliminary results with DW and dynamic enhanced MRI in a much larger patient group.

ACKNOWLEDGMENTS

We thank Prof. Dr. Vincent Grégoire and Ir. John Lee from Université Catholique de Louvain for their kind permission to use the signal-to-background algorithm for ^{18}F-FDG PET delineation. This work was partly supported by grants from the Research Foundation–Flanders, the Flemish League against Cancer, the Belgian Foundation against Cancer, and the Clinical Research Fund of the University Hospitals Leuven. Piet Dirix is a research assistant (aspirant) of the Research Foundation–Flanders. The study was presented at ESTRO 27, September 14–18, 2008, Göteborg, Sweden.

REFERENCES

1. Galvin JM, De Neve W. Intensity modulating and other radiation therapy devices for dose painting. *J Clin Oncol.* 2007;25:924–930.
2. Ling CC, Humm J, Larson S, et al. Towards multidimensional radiotherapy: biological imaging and biological conformality. *Int J Radiat Oncol Biol Phys.* 2000;47:551–560.
3. Nuyts S. Defining the target for radiotherapy of head and neck cancer. *Cancer Imaging.* 2007;7(suppl):S50–S55.
4. Grégoire V, Haustermans K, Geets X, Roels S, Lonneux M. PET-based treatment planning in radiotherapy: a new standard? *J Nucl Med.* 2007;48(suppl):68S–77S.
5. Daisne J-F, Duprez T, Weynand B, et al. Tumor volume in pharyngolaryngeal squamous cell carcinoma: comparison at CT, MR imaging, and FDG-PET and validation with surgical specimen. *Radiology.* 2004;233:93–100.
6. Schwartz DL, Ford E, Rajendran J, et al. FDG-PET/CT imaging for preradiotherapy staging of head-and-neck squamous cell carcinoma. *Int J Radiat Oncol Biol Phys.* 2005;61:129–136.
7. Schwartz DL, Ford EC, Rajendran J, et al. FDG-PET/CT-guided intensity modulated head and neck radiotherapy: a pilot investigation. *Head Neck.* 2005;27:478–487.
8. Madani I, Duthoy W, Derie C, et al. Positron emission tomography-guided, focal-dose escalation using intensity-modulated radiotherapy for head and neck cancer. *Int J Radiat Oncol Biol Phys.* 2007;68:126–135.
9. Koh WJ, Rasey JS, Evans ML, et al. Imaging of hypoxia in human tumors with [F-18] fluoromisonidazole. *Int J Radiat Oncol Biol Phys.* 1992;22:199–212.
10. Rajendran JG, Schwartz DL, O'Sullivan J, et al. Tumor hypoxia imaging with [F-18] fluoromisonidazole positron emission tomography in head and neck cancer. *Clin Cancer Res.* 2006;12:5435–5441.
11. Thorwarth D, Eschmann S-M, Paulsen F, Alber M. Hypoxia dose painting by numbers: a planning study. *Int J Radiat Oncol Biol Phys.* 2007;68:291–300.
12. Lee NY, Mechalakos JG, Nehmeh S, et al. Fluorine-18-labeled fluoromisonidazole positron emission and computed tomography-guided intensity-modulated radiotherapy for head and neck cancer: a feasibility study. *Int J Radiat Oncol Biol Phys.* 2008;70:2–13.
13. Le Bihan D. Molecular diffusion, tissue microdynamics and microstructure. *NMR Biomed.* 1995;8:375–386.
14. Vandecaveye V, De Keyzer F, Nuyts S, et al. Detection of head and neck squamous cell carcinoma with diffusion-weighted MRI after (chemo)radiotherapy: correlation between radiologic and histopathologic findings. *Int J Radiat Oncol Biol Phys.* 2007;67:960–971.
15. Vandecaveye V, De Keyzer F, Vander Poorten V, et al. Head and neck squamous cell carcinoma: value of diffusion-weighted MR imaging for nodal staging. *Radiology.* 2009;251:131–146.
16. Dirix P, De Keyzer F, Vandecaveye V, Stroobants S, Hermans R, Nuyts S. Diffusion-weighted magnetic resonance imaging to evaluate major salivary gland function before and after radiotherapy. *Int J Radiat Oncol Biol Phys.* 2008; 71:1365–1371.
17. Patterson DM, Padhani AR, Collins DJ. Technology insight: water diffusion MRI—a potential new biomarker of response to cancer therapy. *Nat Clin Pract Oncol.* 2008;5:220–233.
18. Padhani AR. Dynamic contrast-enhanced MRI in clinical oncology: current status and future directions. *J Magn Reson Imaging.* 2002;16:407–422.
19. Zahra MA, Hollingsworth KG, Sala E, Lomas DJ, Tan LT. Dynamic contrast-enhanced MRI as a predictor of tumor response to radiotherapy. *Lancet Oncol.* 2007;8:63–74.
20. Nuyts S, Dirix P, Clement PM, et al. Impact of adding concomitant chemotherapy to hyperfractionated accelerated radiotherapy for advanced head-and-neck squamous cell carcinoma. *Int J Radiat Oncol Biol Phys.* 2009;73:1088–1095.
21. Daisne J-F, Sibomana M, Bol A, Doumont T, Lonneux M, Grégoire V. Tridimensional automatic segmentation of PET volumes based on measured source-to-background ratios: influence of reconstruction algorithms. *Radiother Oncol.* 2003;69:247–250.
22. Rajendran JG, Krohn KA. Imaging tumor hypoxia. In: Bailey DL, Townsend DW, Valk PE, Maisey MN, eds. *Positron Emission Tomography, Principles and Practice.* London, U.K.: Springer-Verlag; 2002.
23. Dirix P, Nuyts S, Vanstraelen B, et al. Post-operative intensity-modulated radiotherapy for malignancies of the nasal cavity and paranasal sinuses. *Radiother Oncol.* 2007;85:385–391.
24. Geets X, Tomsej M, Lee JA, et al. Adaptive biological image-guided IMRT with anatomic and functional imaging in pharyngo-laryngeal tumors: impact on target volume delineation and dose distribution using helical tomotherapy. *Radiother Oncol.* 2007;85:105–115.
25. Rasch C, Keus R, Pameijer FA, et al. The potential impact of CT-MRI matching on tumor volume delineation in advanced head and neck cancer. *Int J Radiat Oncol Biol Phys.* 1997;39:841–848.
26. Geets X, Daisne J-F, Arcangeli S, et al. Inter-observer variability in the delineation of pharyngo-laryngeal tumor, parotid glands and cervical spinal cord: comparison between CT-scan and MRI. *Radiother Oncol.* 2005;77:25–31.

27. Allal AS, Slosman DO, Kebdani T, Allaoua M, Lehmann W, Dulguerov P. Prediction of outcome in head-and-neck cancer patients using the standardized uptake value of 2-[^{18}F]-fluoro-2-deoxy-D-glucose. *Int J Radiat Oncol Biol Phys.* 2004;59:1295–1300.
28. Schwartz DL, Rajendran J, Yueh B, et al. FDG-PET prediction of head and neck squamous cell cancer outcomes. *Arch Otolaryngol Head Neck Surg.* 2004;130: 1361–1367.
29. Vernon MR, Maheshwari M, Schultz CJ, et al. Clinical outcomes of patients receiving integrated PET/CT-guided radiotherapy for head and neck carcinoma. *Int J Radiat Oncol Biol Phys.* 2008;70:678–684.
30. Soto DE, Kessler ML, Piert M, Eisbruch A. Correlation between pretreatment FDG-PET biological target volume and anatomical location of failure after radiation therapy for head and neck cancers. *Radiother Oncol.* 2008;89: 13–18.
31. Nordsmark M, Bentzen SM, Rudat V, et al. Prognostic value of tumor oxygenation in 397 head and neck tumors after primary radiation therapy: an international multi-center study. *Radiother Oncol.* 2005;77:18–24.
32. Eschmann S-M, Paulsen F, Reimold M, et al. Prognostic impact of hypoxia imaging with ^{18}F-misonidazole PET in non-small cell lung cancer and head and neck cancer before radiotherapy. *J Nucl Med.* 2005;46:253–260.
33. Rischin D, Hicks RJ, Fisher R, et al. Prognostic significance of [^{18}F]-misonidazole positron emission tomography-detected tumor hypoxia in patients with advanced head and neck cancer randomly assigned to chemoradiation with or without tirapazamine: a substudy of Trans-Tasman Radiation Oncology Group Study 98.02. *J Clin Oncol.* 2006;24:2098–2104.
34. Eschmann S-M, Paulsen F, Bedeshem C, et al. Hypoxia-imaging with ^{18}F-misonidazole and PET: changes of kinetics during radiotherapy of head-and-neck cancer. *Radiother Oncol.* 2007;83:406–410.
35. Popple RA, Ove R, Shen S. Tumor control probability for selective boosting of hypoxic subvolumes, including the effect of reoxygenation. *Int J Radiat Oncol Biol Phys.* 2002;54:921–927.
36. Thorwarth D, Eschmann S-M, Paulsen F, Alber M. A model of reoxygenation dynamics of head-and-neck tumors based on serial ^{18}F-fluoromisonidazole positron emission tomography investigations. *Int J Radiat Oncol Biol Phys.* 2007;68:515–521.
37. Lin Z, Mechalakos J, Nehmeh S, et al. The influence of changes in tumor hypoxia on dose-painting treatment plans based on ^{18}F-FMISO positron emission tomography. *Int J Radiat Oncol Biol Phys.* 2008;70:1219–1228.
38. Hamstra DA, Lee KC, Moffat BA, et al. Diffusion magnetic resonance imaging: an imaging treatment response biomarker to chemoradiotherapy in a mouse model of squamous cell cancer of the head and neck. *Transl Oncol.* 2008;1:187–194.
39. Pickles MD, Manton DJ, Lowry M, Turnbull LW. Prognostic value of pretreatment DCE-MRI parameters in predicting disease free and overall survival for breast cancer patients undergoing neoadjuvant chemotherapy. *Eur J Radiol.* June 20, 2008 [Epub ahead of print].
40. Hermans R, Meijerink M, Van den Bogaert W, Rijnders A, Weltens C, Lambin P. Tumor perfusion rate determined noninvasively by dynamic computed tomography predicts outcome in head-and-neck cancer after radiotherapy. *Int J Radiat Oncol Biol Phys.* 2003;57:1351–1356.